Supplemental Materials

Molecular Biology of the Cell

Masuda and Toda

Supplemental Table S1. *S. pombe* strains used in this study.

Strain name	Genotype (all strains contain *leu1-32 ura4-D18*)	Figure used
HR2157	*h⁻ mzt1-T27W-hphR lys1-131 his7*	1A, S1A
HR2391	*h⁺ gfh1Δ::kanR his2*	1A, S1A-B, S1D
HR2077	*h⁺ mod21Δ::kanR ade6-216*	1A, S1A-B, S1D
HR2239	*h⁺ alp16Δ::kanR*	1A, S1A-B, S1D-E
HR2377	*h⁻ kanR-GFP-alp16⁺ aur1R-Pnda3-mCh-atb2 sid4⁺-mRFP-natR*	1B
HR2378	*h⁻ kanR-GFP-mod21⁺ aur1R-Pnda3-mCh-atb2 sid4⁺-mRFP-natR*	1B
HR2379	*h⁻ kanR-GFP-gfh1⁺ aur1R-Pnda3-mCh-atb2 sid4⁺-mRFP-natR*	1B
HR2400	*h⁻ alp16Δ::ura4⁺ kanR-GFP-mod21⁺ aur1R-Pnda3-mCh-atb2 sid4⁺-mRFP-natR*	1B
HR2404	*h⁻ alp16Δ::ura4⁺ kanR-GFP-gfh1⁺ aur1R-Pnda3-mCh-atb2 sid4⁺-mRFP-natR*	1B
HR2408	*h⁻ gfh1Δ::hphR kanR-GFP-alp16⁺ aur1R-Pnda3-mCh-atb2 sid4⁺-mRFP-natR*	1B
HR2412	*h⁻ gfh1Δ::hphR kanR-GFP-mod21⁺ aur1R-Pnda3-mCh-atb2 sid4⁺-mRFP-natR*	1B
HR2420	*h⁻ mod21Δ::hphR kanR-GFP-gfh1⁺ aur1R-Pnda3-mCh-atb2 sid4⁺-mRFP-natR*	1B
HR2416	*h⁻ mod21Δ::hphR kanR-GFP-alp16⁺ aur1R-Pnda3-mCh-atb2 sid4⁺-mRFP-natR*	1B
HR2193	*h⁻ kanR-GFP-alp4⁺ aur1R-Pnda3-mCh-atb2 sid4⁺-mRFP-natR*	2A, 2C, 7B, S4, S5
HR2298	*h⁻ alp16Δ::ura4⁺ kanR-GFP-alp4⁺ aur1R-Pnda3-mCh-atb2 sid4⁺-mRFP-natR*	2A, 2C, 7B, S4, S5
HR2328-1	*h⁻ hphR-GFP-mzt1⁺ aur1R-Pnda3-mCh-atb2 sid4⁺-mRFP-natR*	2B, 2D, 7B, S5
HR2329-2	*h⁻ alp16Δ::ura4⁺ hphR-GFP-mzt1⁺ aur1R-Pnda3-mCh-atb2 sid4⁺-mRFP-natR*	2B, 2D, 7B, S5
HR3152	*h⁺ aur1R-Pnda3-GFP-atb2 sid4⁺-mRFP-natR lys1-131 his2*	2E, S3
HR3154	*h⁺ alp16Δ::ura4⁺ aur1R-Pnda3-GFP-atb2 sid4⁺-mRFP-natR lys1-131 his2*	2E, S3
HR2488	*h⁻ kanR-GFP-alp4⁺ aur1R-Pnda3-mCh-atb2*	2F, S2A
HR2390	*h⁻ mod21Δ::kanR kanR-GFP-alp4⁺ aur1R-Pnda3-mCh-atb2*	2F
HR2387	*h⁺ gfh1Δ::kanR kanR-GFP-alp4⁺ aur1R-Pnda3-mCh-atb2 his2*	2F
HR2300	*h⁻ alp16Δ::ura4⁺ kanR-GFP-alp4⁺ aur1R-Pnda3-mCh-atb2*	2F, S2A
HR2396	*h⁻ hphR-GFP-mzt1⁺ aur1R-Pnda3-mCh-atb2*	2F
HR2381	*h⁻ gfh1Δ::kanR hphR-GFP-mzt1⁺ aur1R-Pnda3-mCh-atb2*	2F
HR2383	*h⁻ mod21Δ::kanR hphR-GFP-mzt1⁺ aur1R-Pnda3-mCh-atb2*	2F
HR2502	*h⁻ alp16Δ::ura4⁺ hphR-GFP-mzt1⁺ aur1R-Pnda3-mCh-atb2*	2F
HR2944	*h⁻ alp16Δ::ura4⁺ aur1R-Pnda3-mCh-atb2 kanR-GFP-alp4⁺ lys1-131*	3A-B, 5A-D, 5F, 7A
HR2952-2	*h⁻ aur1R-Pnda3-mCh-atb2 kanR-GFP-alp4⁺ lys1-131*	3B, 5A-D, 5F, 7A
HR3221-2	*h⁻ Ch16 (ade6-M216) ade6-M210 his2*	3C
HR3224-1	*h⁺ Ch16 (ade6-M216) alp16Δ::ura4⁺ ade6-M210 his2*	3C
HR3237-1	*h⁻ Ch16 (ade6-M216) mad2Δ::leu1⁺ alp16Δ::ura4⁺ ade6-M210*	3C
HR3239-2	*h⁻ Ch16 (ade6-M216) mad2Δ::leu1⁺ ade6-M210*	3C
HR2828	*h⁻ kanR-GFP-alp16 aur1R-Pnda3-mCh-atb2 sid4⁺-mRFP-natR*	4A
HR2867	*h⁻ hphR-GBP-pcp1⁺ kanR-GFP-alp16 aur1R-Pnda3-mCh-atb2 sid4⁺-mRFP-natR*	4A
HR2824	*h⁺ kanR-GFP-alp16⁺ natR-mCherry-alp4⁺ his2*	4B
HR2853	*h⁻ hphR-GBP-pcp1⁺ kanR-GFP-alp16⁺ natR-mCherry-alp4⁺ his2*	4B

HR2957	*h⁻ alp16Δ::ura4⁺ lys1⁺-P3nmt1-alp16 aur1R-Pnda3-mCh-atb2 kanR-GFP-alp4⁺*	5A-D, 5F
HR2958	*h⁻ alp16Δ::ura4⁺ lys1⁺-P41nmt1-alp16 aur1R-Pnda3-mCh-atb2 kanR-GFP-alp4⁺*	5A-D
HR2959	*h⁻ alp16Δ::ura4⁺ lys1⁺-P81nmt1-alp16 aur1R-Pnda3-mCh-atb2 kanR-GFP-alp4⁺*	5A-D
HR3078	*h⁻ alp16Δ::ura4⁺ kanR-GFP-mod21⁺ lys1⁺-P3nmt1-alp16 aur1R-Pnda3-mCh-atb2*	5E
HR3080	*h⁻ alp16Δ::ura4⁺ kanR-GFP-gfh1⁺ lys1⁺-P3nmt1-alp16 aur1R-Pnda3-mCh-atb2*	5E
HR3132	*h⁻ alp16Δ::ura4⁺ gfh1Δ::hphR lys1⁺-P3nmt1-alp16 aur1R-Pnda3-mCh-atb2 kanR-GFP-alp4⁺*	5F
HR3135	*h⁻ alp16Δ::ura4⁺ gfh1Δ::hphR mod21Δ::kanR lys1⁺-P3nmt1-alp16 aur1R-Pnda3-mCh-atb2 kanR-GFP-alp4⁺*	5F
HR1758	*h⁺ aur1R-Pnda3-mCh-atb2 sid4⁺-mRFP-natR lys1-131 his2*	6A
HR2124-33	*h⁺ mzt1-T27W-hphR aur1R-Pnda3-mCh-atb2 sid4⁺-mRFP-natR lys1-131 his2*	6A
HR3021	*h⁺ mzt1-T27W-hphR lys1⁺-P3nmt1-alp16 aur1R-Pnda3-mCh-atb2 sid4⁺-mRFP-natR his2*	6A
HR3024	*h⁻ mzt1-T27W-hphR lys1⁺-P41nmt1-alp16 aur1R-Pnda3-mCh-atb2 sid4⁺-mRFP-natR*	6A
HR3206	*mzt1Δ-natR/+ lys1⁺-P3nmt1-alp16/lys1⁺-P3nmt1-alp16 ade6-M210/ade6-M216 his2/+*	6B
HR3115	*h⁻ lys1⁺-P41nmt1-mzt1 aur1R-Pnda3-mCh-atb2 kanR-GFP-alp4⁺*	7A
HR3117	*h⁻ alp16Δ::ura4⁺ lys1⁺-P41nmt1-mzt1 aur1R-Pnda3-mCh-atb2 kanR-GFP-alp4⁺*	7A
HR2978-2	*h⁻ kanR-GFP-alp4⁺ natR-mCherry-mzt1⁺*	7C
HR3226	*h⁻ alp4-1891*	S1B-C
HR3230	*h⁺ alp4-1891 gfh1Δ::kanR his2*	S1C
HR3227-2	*h⁻ alp4-1891 mod21Δ::kanR*	S1C
JCF1206	*h⁺ ade6-216*	S1D
HRT01	*h⁻*	S1E
HR2353	*h⁻ gfh1Δ::kanR ade6-216*	S1E
HR2354	*h⁻ mod21Δ::kanR ade6-210*	S1E
HR2355	*h⁻ alp16Δ::natR gfh1Δ::kanR mod21Δ::kanR ade6-210*	S1E
HR2238	*h⁻ alp16Δ::ura4⁺*	S1E
HR3321	*h⁻ kanR-GFP-alp4⁺ sid4⁺-mRFP-natR*	S2B-C, S2E-F, S2H
HR3322	*h⁻ alp16Δ::ura4⁺ kanR-GFP-alp4⁺ sid4⁺-mRFP-natR*	S2B-C, S2E-F, S2H
HR3323	*h⁻ hphR-GFP-mzt1⁺ sid4⁺-mRFP-natR*	S2D-E, S2G, S2I
HR3324	*h⁻ alp16Δ::ura4⁺ hphR-GFP-mzt1⁺ sid4⁺-mRFP-natR*	S2D-E, S2G, S2I

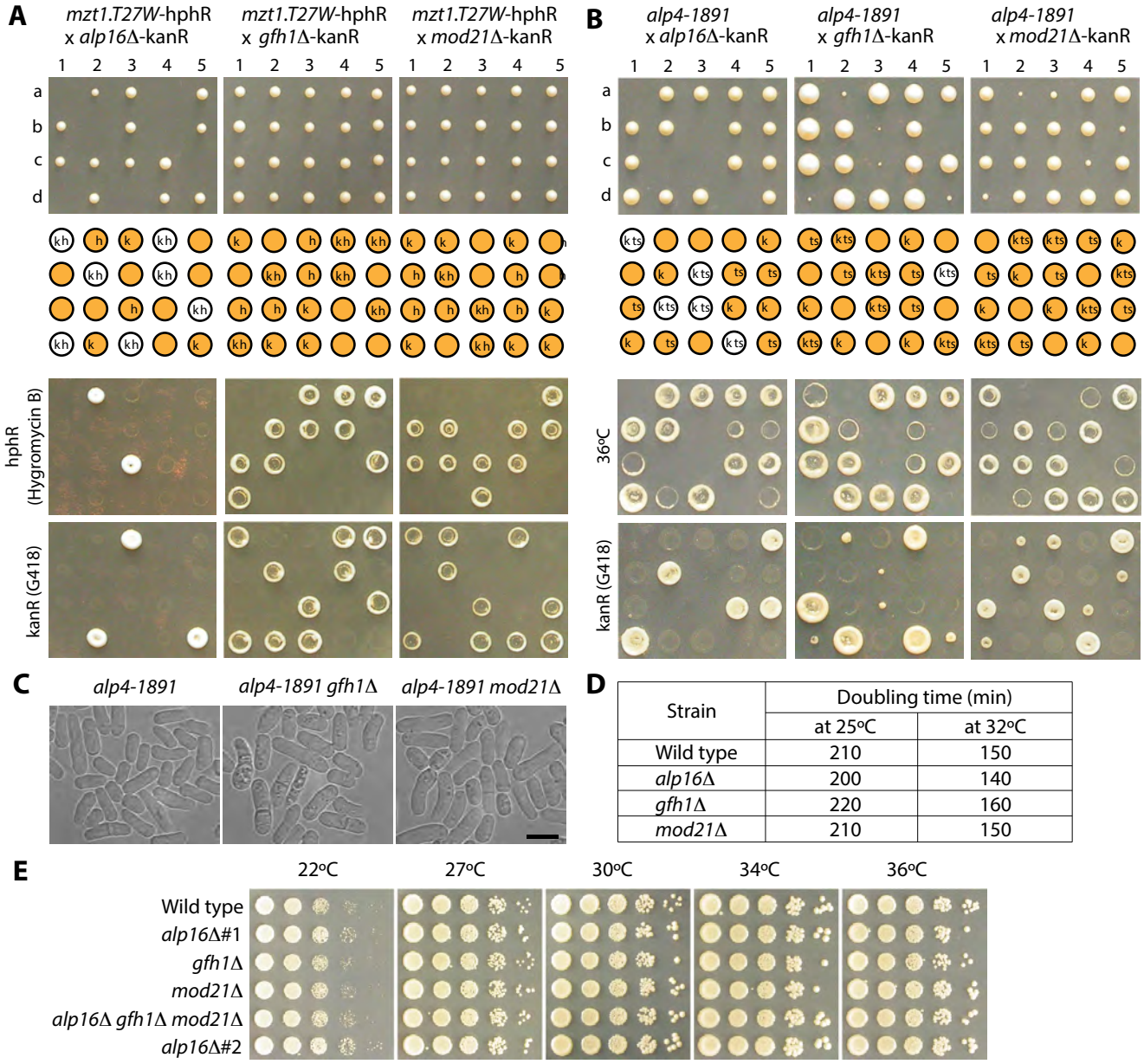

Strain	Doubling time (min)	
	at 25ºC	at 32ºC
Wild type	210	150
alp16Δ	200	140
gfh1Δ	220	160
mod21Δ	210	150

Supplemental Figure S1. *alp16Δ* is synthetic lethal with *mzt1-T27W* and *alp4-1891*.
(A) *alp16Δ* is synthetic lethal with the *mzt1-T27W* mutation. Diploid cells obtained from crosses between *mzt1-T27W*-hphR and *gfh1Δ*-kanR, *mod21Δ*-kanR, or *alp16Δ*-kanR were sporulated and individual spores (a-d) in each ascus (1-5) were dissected on YES plates. Viable spores were replica-plated on YES plates containing G418 or hygromycin B and incubated at 27ºC. The drug resistance of viable spores (orange circle) and the predicted resistance of nonviable spores (white circle) are shown: k, kanR (resistance to G418); and h, hphR (resistance to hygromycin B).
(B) *alp16Δ* is synthetic lethal with *alp4-1891* mutation. Diploid cells obtained from crosses between *alp4-1891* and *gfh1Δ*-kanR, *mod21Δ*-kanR, or *alp16Δ*-kanR were sporulated and individual spores (a-d) in each ascus (1-5) were dissected on YES plates. Viable spores were replica-plated on YES plates and YES plates containing G418, and incubated at 36ºC and 27ºC, respectively. k, kanR (resistance to G418); and ts, temperature-sensitive. (C) *alp4-1891*, *alp4-1891 gfh1Δ*, and *alp4-1891 mod21Δ* cells grown at 27ºC are shown. Scale bar, 10 µm. (D) Doubling time of *alp16Δ*, *gfh1Δ*, and *mod21Δ* cells grown in YES at 25 and 32ºC. (E) Serial dilution spot assay of *alp16Δ*, *gfh1Δ*, *mod21Δ*, and *alp16Δ gfh1Δ mod21Δ* cells. The cells were spotted onto YES plates and incubated for 3 days at various temperatures. *alp16Δ*#1, *alp16Δ::kanR, and alp16Δ*#2, *alp16Δ::ura4*$^{+}$.

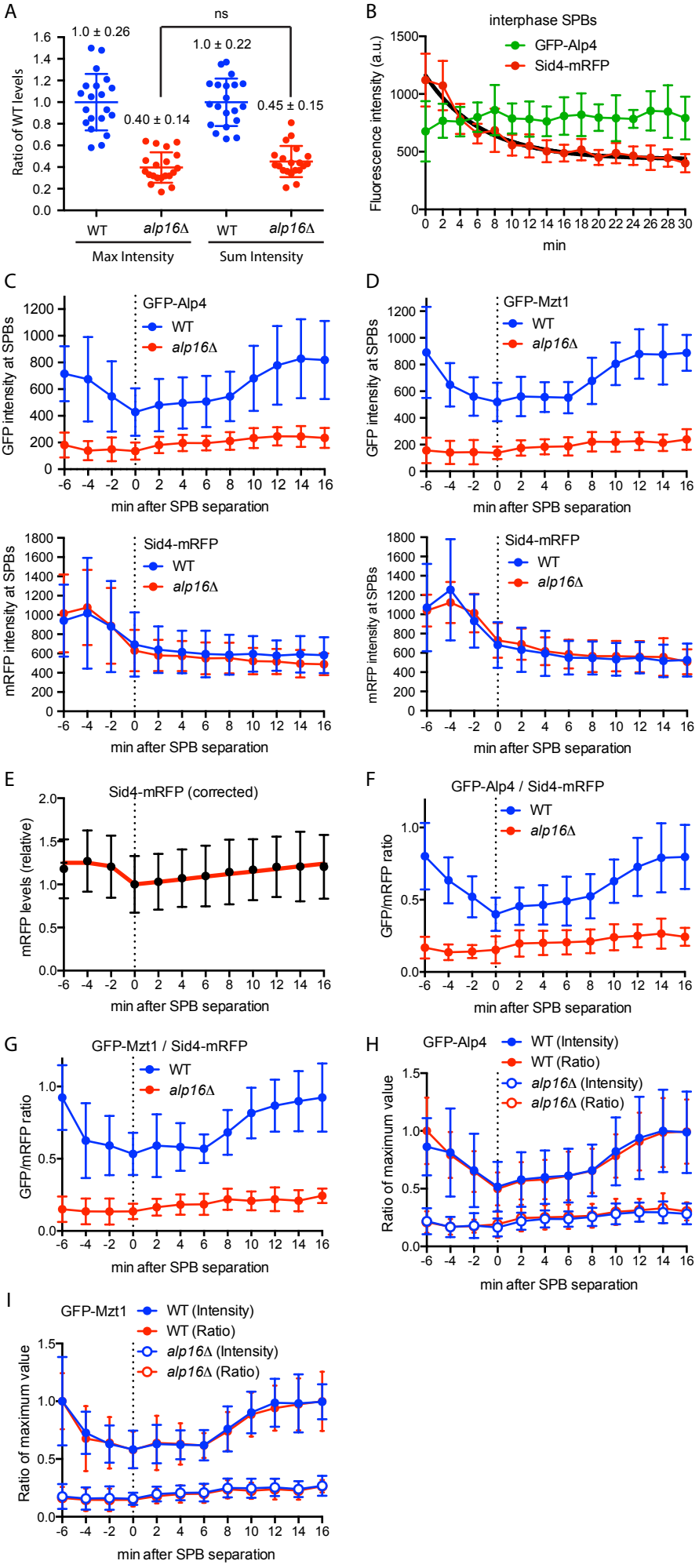
A
ns
1.0 ± 0.26
1.0 ± 0.22
0.40 ± 0.14
0.45 ± 0.15
Ratio of WT levels
WT
alp16Δ
WT
alp16Δ
Max Intensity
Sum Intensity
B
interphase SPBs
GFP-Alp4
Sid4-mRFP
Fluorescence intensity (a.u.)
min
C
GFP-Alp4
WT
alp16Δ
GFP intensity at SPBs
min after SPB separation
D
GFP-Mzt1
WT
alp16Δ
GFP intensity at SPBs
min after SPB separation
Sid4-mRFP
WT
alp16Δ
mRFP intensity at SPBs
min after SPB separation
Sid4-mRFP
WT
alp16Δ
mRFP intensity at SPBs
min after SPB separation
E
Sid4-mRFP (corrected)
mRFP levels (relative)
min after SPB separation
F
GFP-Alp4 / Sid4-mRFP
WT
alp16Δ
GFP/mRFP ratio
min after SPB separation
G
GFP-Mzt1 / Sid4-mRFP
WT
alp16Δ
GFP/mRFP ratio
min after SPB separation
H
GFP-Alp4
WT (Intensity)
WT (Ratio)
alp16Δ (Intensity)
alp16Δ (Ratio)
Ratio of maximum value
min after SPB separation
I
GFP-Mzt1
WT (Intensity)
WT (Ratio)
alp16Δ (Intensity)
alp16Δ (Ratio)
Ratio of maximum value
min after SPB separation

Supplemental Figure S2. Analysis of fluorescence signal intensity.
(A) Quantification of fluorescence intensity. GFP-Alp4^{GCP2} intensities at 20 SPBs of 10 mitotic spindles of < 3.5 μm long in wild type and *alp16Δ* cells were measured from either max intensity projection images or sum intensity projection images. The highest absolute signal intensities at SPB regions were obtained from maximum intensity projection images. Average signal intensities in the regions without cells were subtracted as background intensities from the maximum intensities. Sum intensity images were obtained from 5 image stacks (with a 0.3 μm stack distance) with the stack containing the highest signal intensity in the middle. A 5x5 pixel ROI with maximum sum intensity was determined at each mitotic SPB. Sum intensities of two 20 x 20 pixel regions around the ROI were used for background subtraction.

(B) Change in fluorescence intensity during time-lapse live imaging. Fluorescence intensities of GFP-Alp4^{GCP2} and Sid4-mRFP at 10 interphase SPBs in wild type cells were measured every 2 min for 30 min using the max intensity projection images. Average intensities from 10 SPBs are plotted against time. Note that GFP intensity does not significantly change during 30 min of observation, whereas mRFP intensity reduces with time exponentially (black line).

(C, D) Comparison of Sid4-mRFP, GFP-Alp4^{GCP2} and GFP-Mzt1 levels at mitotic SPBs in wild type and *alp16Δ* cells by time-lapse live imaging. Fluorescence signals from wild type and *alp16Δ* cells containing Sid4-mRFP and GFP-Alp4^{GCP2} (C) or GFP-Mzt1 (D) were recorded every 2min for 30 min. Mitotic spindles formed at 2-6 min after the start of observation were selected for measurement of fluorescence intensity (N = 12 for GFP-Alp4^{GCP2} Sid4-mRFP cells and N = 9 for GFP-Mzt1 Sid4-mRFP cells). Sid4-mRFP levels at mitotic SPBs were similar in wild type and *alp16Δ* cells, and decreased with time. In contrast, GFP-Alp4^{GCP2} and GFP-Mzt1 levels were higher in wild type cells compared to those in *alp16Δ* cells.

(E) Average change in Sid4-mRFP levels during mitosis. Sid4-mRFP levels of all cells analysed in (C) and (D) were corrected using the decay curve shown in (B), and averaged. The mRFP levels relative to those at time 0 (at SPB separation) were plotted against time. Note that Sid4-mRFP levels reduce by 25% at SPB separation, and then increase linearly during mitosis up to the interphase levels.

(F, G) Reanalysis of data shown in (C) and (D) using the ratio of GFP-Alp4^{GCP2} and GFP-Mzt1 to corrected Sid4-mRFP levels at mitotic SPBs. Sid4-mRFP levels were used as internal controls to compare GFP-Alp4^{GCP2} and GFP-Mzt1 levels in wild type and *alp16Δ* cells. The mRFP levels at each SPB at each time point were first corrected using the decay curve shown in (B), and then corrected to the level at time 0 (at SPB separation) by the ratio of average mRFP signal at that time point to average mRFP signal at time 0 using the data shown in (E). The ratio of GFP to the modified mRFP levels are shown.

(H, I) Comparison of data obtained with and without the internal controls. To compare the data shown in (C) and (D) with the data shown in (F) and (G), GFP-Alp4^{GCP2} and GFP-Mzt1 intensities are plotted against time as ratios of the maximum intensity in wild type cells, and GFP-Alp4^{GCP2}/Sid4-mRFP and GFP-Mzt1/Sid4-mRFP ratios are plotted against time as ratios of the maximum GFP/mRFP ratio in wild type cells. Note that almost identical results are obtained by the two methods.

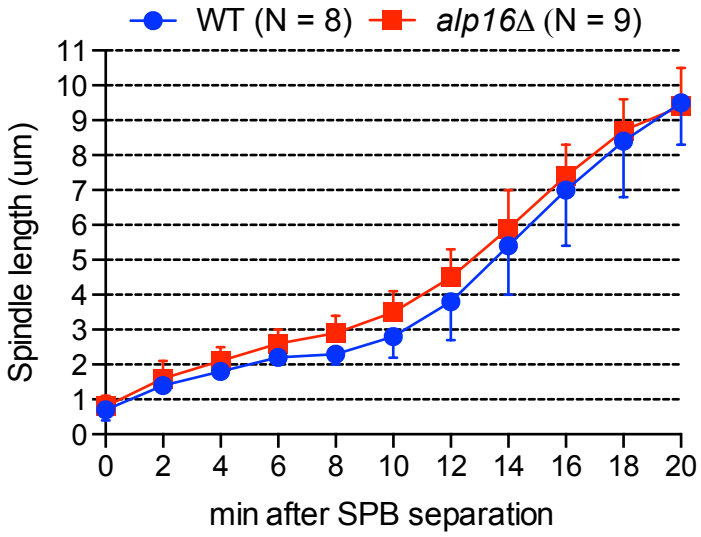

Supplemental Figure S3. *alp16Δ* cells do not show a delay in mitotic progression. Average spindle lengths in wild-type and *alp16Δ* cells expressing GFP-Atb2 and Sid4-mRFP were plotted against time after SPB separation from the time-lapse live images used for Figure 1F. Note that in wild type and *alp16Δ* cells, anaphase starts on average 10 min after SPB separation with spindles of around 3 μm in length.

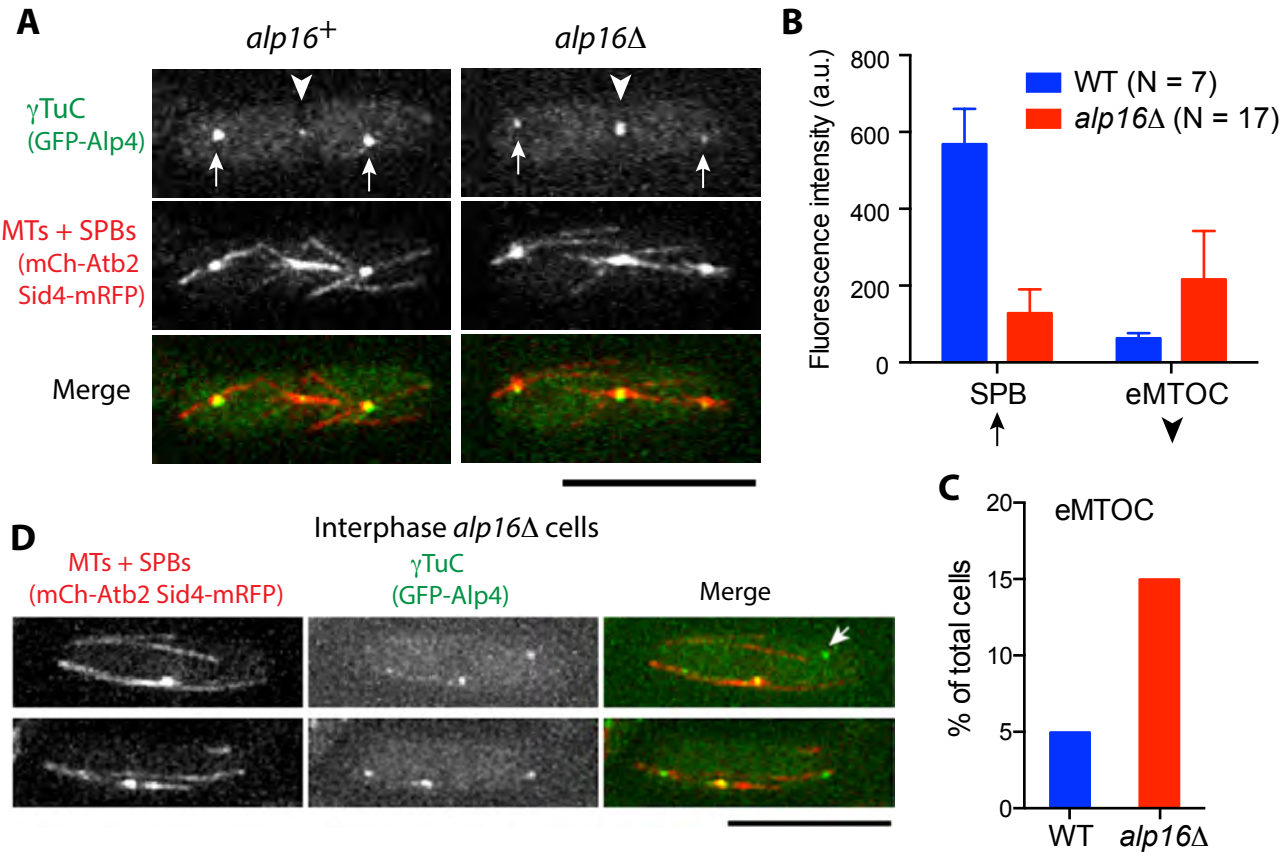

Supplemental Figure S4. Phenotypes of *alp16Δ* cells observed at the M/I transition and interphase. (A) γTuC levels at the eMTOC are increased in *alp16Δ* cells. Wild type and *alp16Δ* cells expressing GFP-Alp4^{GCP2}, mCh-Atb2, and Sid4-mRFP were observed for eMTOC formation. Arrows show the position of the SPB, and arrowheads show the position of the eMTOC. Scale bar, 10 μm. (B) Quantification of GFP-Alp4^{GCP2} levels at SPBs and eMTOCs. (C) Quantification of wild type and *alp16Δ* cells showing eMTOCs. Cells were grown asynchronously to mid-log phase for observation. N >150. (D) Interphase *alp16Δ* cells showing extra γTuC dots on or off cytoplasmic microtubules. Arrow indicates a γTuC dot that does not bind to microtubules. Scale bar, 10 μm.

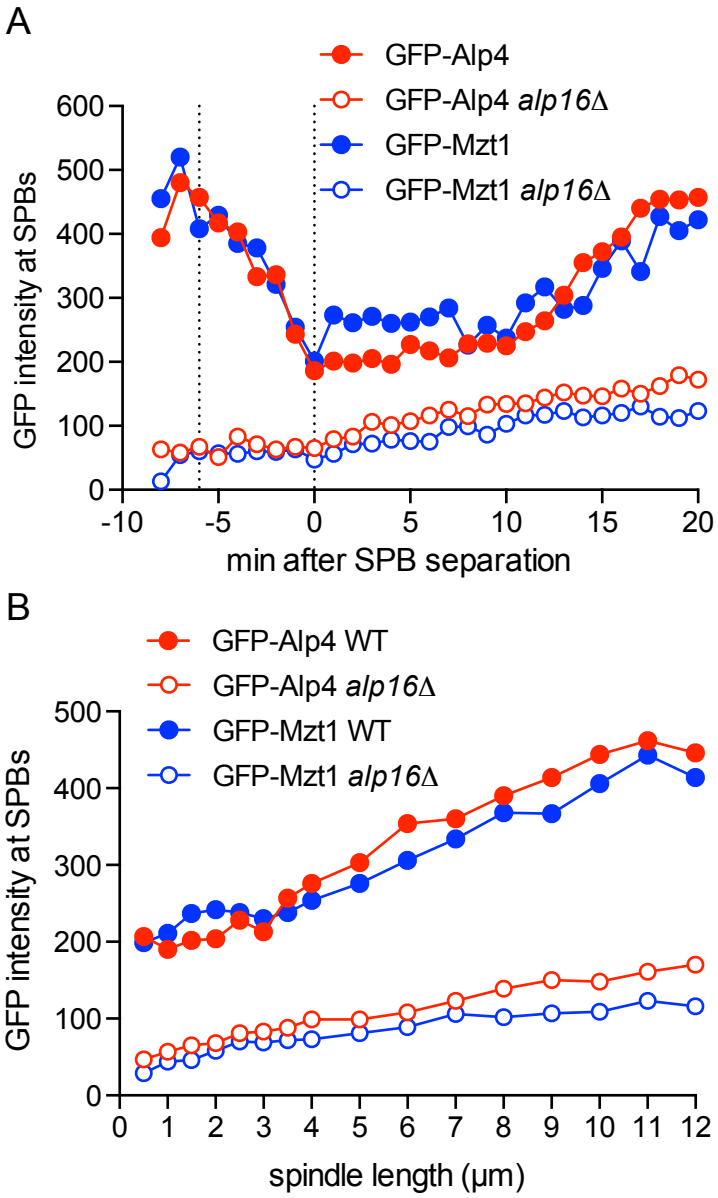

Supplemental Figure S5. Comparison of GFP-Alp4^{GCP2} and GFP-Mzt1 levels.
Average intensities of GFP-Alp4^{GCP2} and GFP-Mzt1 signal in wild type and *alp16Δ* cells were plotted against time after SPB separation (A) and spindle length (B) from the data used for Figures 1D and 1E. Note that the signal intensity of GFP-Mzt1 is higher than GFP-Alp4^{GCP2} only at early M-phase.